HHS Public Access

Author manuscript

ACS Chem Biol. Author manuscript; available in PMC 2019 February 15.

Published in final edited form as:

ACS Chem Biol. 2017 March 17; 12(3): 635–642. doi:10.1021/acschembio.6b01001.

Chemoproteomic profiling of acetanilide herbicides reveals their role in inhibiting fatty acid oxidation

Jessica L. Counihan[1], **Megan Duckering**[1], **Esha Dalvie**[1], **Wan-min Ku**[1], **Leslie A. Bateman**[1], **Karl J. Fisher**[1], and **Daniel K. Nomura**[*,1]

[1]Departments of Chemistry, Molecular and Cell Biology, and Nutritional Sciences and Toxicology, 127 Morgan Hall, University of California, Berkeley, Berkeley, CA 94720

Abstract

Acetanilide herbicides are among the most widely used pesticides in the United States, but their toxicological potential and mechanisms remain poorly understood. Here, we have used chemoproteomic platforms to map proteome-wide cysteine reactivity of acetochlor (AC), the most widely used acetanilide herbicide, *in vivo* in mice. We show that AC directly reacts with >20 protein targets *in vivo* in mouse liver, including the catalytic cysteines of several thiolase enzymes involved in mitochondrial and peroxisomal fatty acid oxidation. We show that the fatty acids that are not oxidized, due to impaired fatty acid oxidation, are instead diverted into other lipid pathways resulting in heightened free fatty acids, triglycerides, cholesteryl esters, and other lipid species in the liver. Our findings show the utility of chemoproteomic approaches for identifying novel mechanisms of toxicity associated with environmental chemicals like acetanilide herbicides.

Keywords

chemoproteomics; activity-based protein profiling; toxicology; pesticides; AC; acetanilides; cysteine reactivity; lipid metabolism; fatty acid oxidation

Current toxicological testing paradigms for pesticides include testing chemicals for various pre-defined phenotypic endpoints such as carcinogenicity, usually through treatment of pesticides at maximum tolerated doses under acute to chronic exposures. While these studies may reveal whether chemicals cause pre-defined toxicological endpoints such as cancer, they may miss more insidious toxicological mechanisms or pathologies, since only a handful of phenotypic endpoints are tested. Another approach towards better understanding the toxicological mechanisms of chemicals is to map their direct on and off-target activity directly in complex biological systems and test for toxicological phenotypes based on the biology known about these targets to provide a more direct route for testing how pesticides may affect health. Chemoproteomic platforms have arisen to tackle this challenge by enabling an approach for identifying direct protein targets of chemicals. Here, we have

[*]correspondence to dnomura@berkeley.edu.

Supporting Information

The Supporting Information is available free of charge on the ACS Publications website at DOI: 10.1021/acschembio.6b01001.

Table S1

Table S2

focused our study on using chemoproteomic platforms to identify the direct targets of acetanilide herbicides, towards understanding potential novel mechanisms of toxicity.

Acetanilide herbicides including metolachlor, alachlor, and acetochlor (AC), are among the most widely used pesticides in the US, with collective usage of nearly >60 million pounds per year, and are primarily used for agricultural weed control[1] (Fig. 1A). Exposure to these agents has been associated with various adverse health effects in rodent models including cancer, developmental and reproductive abnormalities, and dysregulation of thyroid and liver function[2], but the mechanisms underlying these or other toxicological effects are poorly understood.

Of particular concern with acetanilide herbicides are their shared electrophilic chloroacetamide scaffolds that may adduct with cysteines within proteins to cause protein dysfunction. Cysteines play important roles in protein function, including enzyme catalysis, post-translational regulation, redox balance, metal binding, and protein-protein interactions[3]. The reactivity of AC with specific cysteines within certain protein targets may thus affect protein function and cause downstream pathologies, but the proteome-wide reactivity of acetanilide herbicides remains unknown.

Here, we have used activity-based protein profiling (ABPP) to map the proteome-wide reactivity of acetanilide herbicides *in vitro* and *in vivo* in mice, towards understanding novel biological and toxicological mechanisms associated with exposure to these agents. ABPP is a chemoproteomic platform that uses activity- or reactivity-based chemical probes to map proteome-wide reactivity, functionality, and ligandability directly in complex proteomes. When used in a competitive manner, electrophilic environmental chemicals like AC can be competed against the binding of reactivity-based probes to ligandable protein hotspots to map their proteome-wide reactivity and direct protein targets[4,5] (Fig. 1B,1C). To discover the direct targets of acetanilide herbicides, we utilized two chemical probes for this study: 1) a broad cysteine-reactive iodoacetamide probe bearing a biorthogonal alkyne handle (iodoacetamide-alkyne or IAyne) and 2) an analog of AC also bearing an alkyne handle (AC-alkyne or ACyne) (Fig. 1B).

To get an initial portrait of whether acetanilide herbicides might disrupt cysteine reactivity, we performed gel-based ABPP studies in which we competed metolachlor, alachlor, or AC against IAyne or ACyne labeling of mouse liver proteome *in vitro*, followed by appendage of a rhodamine-azide tag by copper-catalyzed click chemistry and visualization of probe-labeled proteins by in-gel fluorescence (Fig. 1C). While metolachlor appears to be inactive, we observed significant inhibition of IAyne and ACyne probe labeling with alachlor and even more so with AC, indicating that these acetanilide herbicides reacted with specific cysteines on specific protein targets *in vitro* in mouse liver proteomes (Fig. 1D). Based on the *in vitro* data, we decided to focus on AC for follow-up *in vivo* studies, since it showed the highest degree of reactivity.

We next investigated AC reactivity *in vivo* in mouse liver. We acutely treated mice with AC and subsequently labeled liver proteomes *ex vivo* with IAyne or ACyne. We show that AC treatment inhibits IAyne and ACyne labeling *ex vivo*, demonstrating that AC shows protein

reactivity *in vivo* in mouse liver (Fig. 1E). To identify these AC protein targets, we next performed ABPP-Multidimensional Protein Identification Technology (ABPP-MudPIT) studies, in which we labeled liver proteomes from vehicle and AC-treated mice with IAyne followed by appendage of biotin-azide by click-chemistry for enrichment and proteomic analysis of probe-labeled proteins (Fig. 1C). Out of 96 protein targets enriched by IAyne labeling, we show 28 distinct targets that exhibit >2-fold inhibition of IAyne labeling *ex vivo* with AC treatment (Fig. 2A). We also performed enrichment and proteomic analysis on ACyne treated mouse liver proteomes and identified 28 distinct enriched protein targets (Fig. 2B). We plotted the overlap between these two proteomic experiments and observed 6 common targets of AC, as these targets are likely to be direct targets of AC itself rather than a potential bioactivated metabolite of AC (Fig. 2C). While these bioactivated metabolites that show cysteine reactivity may be of interest, we wanted to focus our efforts for this study on targets that could be more easily validated with the parent pesticide AC. Interestingly, 5 of these 6 targets are involved in fatty acid metabolism, including Scp2, Acaa2, Acaa1b, Acat1, and Acsf2, of which Scp2, Acaa2, Acaa1b, and Acat1 are all part of the same thiolase family of enzymes and Acsf2 is a fatty acyl CoA synthetase[6]. We decided to follow-up on these 5 specific targets of AC.

To identify the specific sites of labeling of AC on these 5 protein targets, we also complemented our ABPP protein pull-down experiments with isotopic tandem orthogonal proteolysis-enabled ABPP (isoTOP-ABPP), in which we labeled mouse liver proteomes from vehicle or AC-treated mice with IAyne, appended a biotin-azide tag bearing an isotopically light (for vehicle-treated) or heavy (for AC-treated) valine and a TEV protease recognition sequence by click-chemistry, avidin-enriched and tryptically digested probe labeled proteins, released probe-modified peptides by TEV protease, and analyzed light to heavy ratios of probe-labeled proteins by quantitative proteomics (Fig. 1C, Fig. 2D). Across all 5 targets, we identified specific IAyne-labeled cysteines that showed >1.5 light-to-heavy (L/H) ratios indicating that these sites were bound by AC. Of particular interest were Acaa2 C92, Acaa1b C123, and Scp2 C94 that showed L/H ratios of 2.7, 1.8, and 2.0, respectively (Fig. 2D, 2E). These particular cysteines are the catalytic cysteines of these enzymes, suggesting that AC treatment *in vivo* inhibited the activity of these enzymes. We further validated these findings by showing competition of AC against IAyne labeling of pure Acaa2, Acaa1b, and Scp2 protein by gel-based ABPP and showing inhibition of Acaa1 and Acaa2 thiolase activity by AC (Fig. 2F, 2G).

Acaa1b, Acaa2, and Scp2 are all degradative thiolases and are critical enzymes in the fatty acid oxidation pathways in both mitochondria (Acaa2) and in long-chain and branched-chain fatty acid oxidation in peroxisomes (Acaa1, Scp2). Genetic deficiencies in these thiolases or of peroxisomal or mitochondrial fatty acid oxidation pathways have been shown to cause liver dysfunction and lipid dysregulation in the form of elevated triacylglycerols, ceramides, and sterols, as well as hepatic steatosis, likely because the fatty acids that are not oxidized are diverted into other lipid metabolism pathways[7–11].

We, thus, postulated that AC treatment, through inhibiting mitochondrial and peroxisomal fatty acid oxidation enzymes, may also cause lipid dysregulation due to the diversion of fatty acids away from oxidation and towards other lipid pools. Consistent with this premise, using

targeted metabolomic platforms, we show that daily subacute treatment of mice with AC leads to heightened levels of fatty acids, neutral lipids, phospholipids, sphingolipids, and sterols in mouse liver normalized to mouse liver weight (Fig. 3A). We further show that these changes in triglycerides and cholesteryl esters are particularly exacerbated upon AC treatment and feeding mice with a high-fat diet (Fig. 3B).

While our steady-state *in vivo* lipidomic data suggested that fatty acids may be diverted towards lipid storage in the liver due to inhibition of fatty acid oxidation enzymes, we further tested this hypothesis by tracing isotopically labeled [U-^{13}C]palmitate in HepG2 hepatocyte cell lines. We demonstrate that AC treatment in HepG2 cells leads to significantly heightened isotopic fatty acid incorporation into fatty acyl carnitines, ceramides, and triacylglycerols, compared to vehicle-treated controls (Fig. 3C).

To further show that the oxidation of fatty acids is inhibited upon AC exposure, we measured the oxygen consumption rate (OCR), a measure of cellular oxygen consumption, mitochondrial respiration, and energy production, in HepG2 hepatocytes. We show that basal OCR is heightened upon exogenous palmitate treatment, but significantly lowered upon AC treatment compared with vehicle-treated controls, to comparable levels as those observed with treatment with a fatty acid oxidation carnitine palmitoyltransferase-1 (CPT-1) inhibitor etomoxir (Fig. 3D). We also inhibited mitochondrial ATP production using oligomycin, and show that both AC and etomoxir treatment impaired OCR, reflecting an impairment of ATP synthesis. We also find impaired OCR in AC and etomoxir-treated cells compared to vehicle-treated controls upon mitochondrial uncoupling with FCCP, which induces maximal mitochondrial respiration. To determine whether AC also impaired OCR from non-mitochondrial sources, such as the peroxisome, HepG2 cells were also treated with mitochondrial respiratory chain inhibitors rotenone and antimycin A. Consistent with the hypothesis that AC exposure leads to inhibition of both mitochondrial and perioxisomal fatty acid oxidation, OCR impairment was also observed with AC, but not with etomoxir, treatment upon addition of mitochondrial respiratory chain inhibitors. Taken together, our data demonstrate that AC inhibits fatty acid oxidation in hepatocytes (Fig. 3D).

Collectively, our data suggest that AC, through inhibiting the catalytic cysteines of key thiolase enzymes Acaa1b, Acaa2, and Scp2 involved in mitochondrial and peroxisomal fatty acid oxidation, leads to an accumulation of fatty acids that are diverted towards synthesis of various other lipid species, including neutral lipids, sphingolipids, triacylglycerols, and cholesteryl esters (Fig. 3E). Our data point to a unique and novel toxicological mechanism associated with exposure to AC, a very highly used herbicide, in which chronic exposure to this agent may exert potential dyslipidemic effects, such as hepatic steatosis. We acknowledge that the doses and routes of exposure used in this study do not necessarily represent the doses and exposure routes encountered in agricultural or home settings. However, AC covalently modifies its targets and chronic and low dose exposure may lead to accumulating inhibition of these targets over time, since protein half-life rather than the half-life of AC *in vivo* will likely dictate the length of inhibition of these targets. It will be of future interest to investigate whether these targets are inhibited *in vivo* from low-dose and chronic AC exposure in drinking water or through inhalation exposures. Furthermore, ABPP as it is used in this study is primarily useful for identifying irreversible and covalent targets

of chemicals, but there may be reversible targets of acetochlor that we missed in our profiling efforts.

From the viewpoint of pesticide toxicological testing, pesticides are oftentimes tested at the maximum tolerated doses for whether they cause toxicity. Here, we used a rather high dose, but far lower than doses that would cause overt toxicity and far lower than the maximum tolerated doses. We envision in the future that chemoproteomic platforms such as ABPP would be integrated into early-stage toxicity testing, rather that applied on chemicals that are already in our environment, towards identifying direct toxicological targets and using these information to fine-tune toxicological endpoints that may be tested for in long-term toxicological testing studies.

Nonetheless, our data here underscore the utility of using chemoproteomic platforms like ABPP to map the direct proteome-wide targets of environmental chemicals towards understanding unique and novel mechanisms of toxicity, particularly for those chemicals that are potentially reactive or can be transformed to reactive metabolites. While testing environmental chemicals for mutagenicity, carcinogenicity, or endocrine disruption are standard toxicological practices, testing whether a chemical inhibits fatty acid oxidation enzymes, and thus whether it alters fatty acid and lipid dynamics, is not part of standard testing and would likely be missed as a toxicological endpoint. By using ABPP platforms, we show here that direct off-targets of environmental chemicals can be identified *in vivo*, enabling more in-depth and broader assessments of toxicities and toxicological mechanisms. We put forth the chemoproteomic strategies described here as a generalizable approach towards testing the toxicity and elucidating toxicological mechanisms of environmental, industrial, and pharmaceutical chemicals.

Methods

Mice.

Male C57BL/6 mice (6–8 weeks old) were acutely (4 hours) or sub-acutely (6 days) exposed by intraperitoneal (ip) injection to 85 mg/kg AC (Sigma #33379) in a vehicle of 18:1:1 PBS:PEG40:ethanol (300 μl per mouse). Mice used in metabolic studies were in a vehicle of 19:1 PBS:PEG40 (300 μl per mouse). Following exposure, mice were sacrificed by cervical dislocation, the liver was immediately removed, and subsequently flash frozen in liquid nitrogen. All animal experiments were conducted in accordance with the guidelines of the Institutional Animal Care and Use Committee of the University of California, Berkeley (AUP R342).

Processing of Mouse Liver Proteomes.

Tissues were homogenized in phosphate buffered saline (PBS) followed by a 1000 × g centrifugation of the homogenate. The resulting supernatant was collected and used for subsequent assays. Protein concentrations were determined by BCA protein assay (Pierce #23225).

Cell Culture, Recombinant Overexpression, and *in situ* [^{13}C]Palmitic Acid Tracing.

HepG2 (ATCC HB-8065) cells were cultured in Eagle's Minimum Essential Medium (EMEM) containing 10% fetal bovine serum (Corning). Substrate-limited Dulbecco's Modified Eagle's Medium (DMEM) containing 0.5 mM glucose (Sigma-Aldrich #G7021), 1 mM GlutaMAX (Life Technologies #35050061), 0.5 mM carnitine (Sigma-Aldrich #C0283), and 1% fetal bovine serum was used for the HepG2 Seahorse studies. FAO Assay Medium for the HepG2 Seahorse studies contained 111 mM NaCl, 4.7 mM KCl, 1.25 mM CaCl2, 2 mM MgSO4, 1.2 mM Na2HPO4, and supplemented on the day of the assay with 2.5 mM glucose, 0.5 mM carnitine, and 5 mM HEPES. Both Seahorse mediums were pH adjusted to 7.4. HEK 293T/17 (ATCC CRL-11268) cells were cultured in DMEM containing 10% fetal bovine serum and 2 mM L-glutamine (Life Technologies) and maintained at 37°C with 5% CO_2. Recombinant cDNA construct containing Scp2 in the SPORT6 vector was purchased from GE Healthcare Dharmacon Inc. and transiently transfected into HEK 293T/17 cells using Lipofectamine 2000 (Life Technologies #11668019). HepG2 cells were treated with 1 mM AC or vehicle for 1 h in serum-free EMEM and then treated for 6 h with 10 μM [^{12}C] or [^{13}C]palmitic acid (Cambridge Isotope Laboratories, Inc.).

Synthesis of ACyne (2-ethyl-N-(hex-5-yn-1-yl)-6-methylaniline).

Chloroacetyl chloride (70.0 mg, 0.625 mmol) was added to a solution of 2-ethyl-N-(hex-5-yn-1-yl)-6-methylaniline (39.5 mg, 0.184 mmol) in dichloromethane. The reaction was stirred, and diisopropylethylamine (300 μL, 1.72 mmol) was added via syringe. The color of the solution quickly turned black and a white vapor arose from the reaction mixture. The reaction was stirred at room temperature for 16 hours. It was then quenched by addition of aqueous sodium bicarbonate, and extracted into ethyl acetate. The organic solvent was removed by rotary evaporation to give the crude product. Purification by silica gel chromatography (20% to 30% ethyl acetate in hexanes) gave the product in 78% yield (39.5 mg)

Characterization of ACyne (2-ethyl-N-(hex-5-yn-1-yl)-6-methylaniline).

^{1}H NMR (500 MHz, $CDCl_3$): δ 7.25 (m, 1H), 7.20 (d, *J* = 6.5 Hz, 1H), 7.13 (d, *J* = 7.5 Hz, 1H), 3.64 (s, 2H), 3.62–3.52 (m, 2H), 2.59–2.50 (m, 2H), 2.23 (s, 3H), 2.19 (dt, *J = 2.5*, 7.0 Hz, 2H), 1.89 (t, *J* = 2.5 Hz, 1H), 1.71–1.64 (m, 2H), 1.55–1.46 (m, 2H), 1.23 (t, *J = 7.5* Hz, 3H).

^{13}C NMR (500 MHz, $CDCl_3$): δ 167.0, 142.1, 136.3, 129.6, 129.3, 127.7, 83.9, 69.1, 50.2, 42.2, 27.0, 26.5, 24.0, 18.9, 18.6, 14.5.

HRMS (ESI+): Expected 292.1463 (M+H), $C_{17}H_{23}ClNO$. Found 292.1465

Gel-based ABPP.

Proteome samples diluted in PBS (50 μg in 50 μl PBS) or pure proteins (5 μg in 50 μl PBS, OriGene Technologies, Inc.) were subjected to vehicle or AC treatment for 30 min at 37°C. Then, IAyne (10 μM, CHESS Gmbh #3187) or ACyne labeling was performed for 30 min at 37°C. Copper-catalyzed azide-alkyne cycloaddition "click chemistry" was performed with

the IAyne or ACyne probe using previously described methods[12,13]. Fluorescent detection was performed by running a 16 cm Protean II xi 10% resolving SDS-PAGE gel system (Bio-Rad) and scanned using a ChemiDoc MP (Bio-Rad Laboratories, Inc.). Inhibition of target labeling was assessed by densitometry using ImageLab software 5.2.1 (Bio-Rad Laboratories, Inc.) and regressions were calculated by Prism (GraphPad Software).

ABPP-MudPIT.

Proteome samples from control- or AC-treated mice were diluted (1 mg in 500 μL PBS), and then labeled with IAyne or ACyne for 1 h at 37°C. Click chemistry was performed by sequential addition of tris(2-carboxyethyl)phosphine (1 mM, Sigma-Aldrich), copper (II) sulfate (1 mM, Sigma-Aldrich), tris[(1-benzyl-1H-1,2,3-triazol-4-yl)methyl]amine (34 μM, Sigma-Aldrich) using previously described methods[12,13]. After the click reactions, proteomes were precipitated by centrifugation at 6500 × g, washed twice in ice-cold methanol, then denatured and re-solubilized by heating in 1.2% SDS/PBS to 85°C for 5 minutes. Insoluble components were precipitated by centrifugation at 6500 × g and the soluble proteome was diluted in 5 ml PBS, for a final concentration of 0.2% SDS. Labeled proteins bound to avidin-agarose beads (170 μL re-suspended beads/sample, Thermo Pierce) while rotating overnight at 4°C. Bead-linked proteins were enriched by washing three times each in PBS and water, re-suspended in 6 M urea/PBS (Sigma-Aldrich), reduced in dithiothreitol (DTT) (1 mM, Sigma-Aldrich), alkylated with iodoacetamide (18 mM, Sigma-Aldrich), then washed and re-suspended in 2 M urea and trypsinized overnight at 37°C while being agitated with 0.5 μg/μl sequencing grade trypsin (Promega). The resulting tryptic peptides were diluted in water and acidified with a final concentration of 5% formic acid (1.2 M, Spectrum). The entire volume was pressure-loaded onto a 250 mm i.d. fused silica capillary tubing packed with 4 cm of Aqua C18 reverse-phase resin (phenomenex #04A-4299), which was previously equilibrated on an Agilent 600 series HPLC using gradient from 100% buffer A to 100% buffer B over 10 min, followed by a 5 min wash with 100% buffer B and a 5 min wash with 100% buffer A. The sample was then attached using a MicroTee PEEK 360 um fitting (Thermo Fisher Scientific #p-888) to a 10 cm laser pulled column of 100 mm fused silica capillary packed with 10 cm Aqua C18 reverse-phase resin, which was previously equilibrated using the same conditions as above. Tryptic peptide samples were analyzed by attaching the loaded sample to an Orbitrap Q Exactive Plus mass spectrometer (Thermo Fisher Scientific) set to run full scan in the range 400–1800 MW, and 15 data-dependent scans at a temperature of 200°C and a spray voltage of 2.75kV. Samples were run using a two-hour gradient from 5% to 80% acetonitrile with 0.1% formic acid at 100 nl/min. Data was extracted in the form of MS2 files using Raw Extractor 1.9.9.2 (Scripps Research Institute) and searched against the Uniprot mouse database using ProLuCID search methodology in IP2 v.3 (Integrated Proteomics Applications, Inc.).

IsoTOP-ABPP.

For isoTOP-ABPP, liver proteomes from vehicle and AC-treated mice were labeled with IAyne (100 μM) for 1 h at room temperature. Proteomes were subsequently treated with isotopically light (control) or heavy (treated) TEV-biotin (100 μM) and copper-catalyzed alkyne-azide cycloaddition (CuAAC) was performed as previously described[13,14]. TEV-biotin was synthesized in our lab per methods previously described[13,15]. Proteins were

precipitated over one hour and pelleted by centrifugation at 6500 × *g*. Proteins were washed 3 times with cold methanol then denatured and resolubilized by heating in 1.2% SDS/PBS to 85° C for 5 min. Insoluble components were precipitated by centrifugation at 6500 × *g* and soluble proteome was diluted in 5 ml PBS, for a final concentration of 0.2% SDS. Labeled proteins were bound to avidinagarose beads (170 μL resuspended beads/sample, Thermo Pierce) while rotating overnight at 4°C. Bead-linked proteins were enriched by washing three times each in PBS and water, then resuspended in 6 M urea/PBS (Sigma-Aldrich) and reduced in dithiothreitol (1 mM, Sigma-Aldrich), alkylated with iodoacetamide (18 mM, Sigma-Aldrich), then washed and resuspended in 2 M urea/PBS with 1 mM calcium chloride and trypsinized overnight with 0.5 μg/μl sequencing grade trypsin (Promega). Tryptic peptides were discarded and beads were washed three times each in PBS and water, then washed with one wash of TEV buffer containing 1 μM DTT. TEV-biotin tag was digested overnight in TEV buffer containing 1 μM DTT and 5 μL Ac-TEV protease at 29°C. Peptides were diluted in water and acidified with final concentration of 5% formic acid (1.2 M, Spectrum).

MS Analysis.

Peptides from proteomic experiments were pressure-loaded onto a 250 mm inner diameter fused silica capillary tubing packed with 4 cm of Aqua C18 reverse-phase resin (Phenomenex # 04A-4299) which was previously equilibrated on an Agilent 600 series HPLC using gradient from 100% buffer A to 100% buffer B over 10 min, followed by a 5 min wash with 100% buffer B and a 5 min wash with 100% buffer A. The samples were then attached using a MicroTee PEEK 360 μm fitting (Thermo Fisher Scientific #p-888) to a 13 cm laser pulled column packed with 10 cm Aqua C18 reverse-phase resin and 3 cm of strong-cation exchange resin for isoTOP-ABPP studies. Samples were analyzed using an Q Exactive Plus mass spectrometer (Thermo Fisher Scientific) using a 5-step Multidimensional Protein Identification Technology (MudPIT) program, using 0 %, 25 %, 50 %, 80 %, and 100 % salt bumps of 500 mM aqeous ammonium acetate and using a gradient of 5–55 % buffer B in buffer A (buffer A: 95:5 water:acetonitrile, 0.1 % formic acid; buffer B 80:20 acetonitrile:water, 0.1 % formic acid). Data was collected in data-dependent acquisition mode with dynamic exclusion enabled (60 s). One full MS (MS1) scan (400–1800 m/z) was followed by 15 MS2 scans (ITMS) of the nth most abundant ions. Heated capillary temperature was set to 200° C and the nanospray voltage was set to 2.75 kV.

Data was extracted in the form of MS1 and MS2 files using Raw Extractor 1.9.9.2 (Scripps Research Institute) and searched against the Uniprot mouse database using ProLuCID search methodology in IP2 v.3 (Integrated Proteomics Applications, Inc)[16]. Cysteine residues were searched with a static modification for carboxyaminomethylation (+57.02146) and up to two differential modifications for methionine oxidation and either the light or heavy TEV tags (+464.28596 or +470.29977, respectively). Peptides were required to have at least one tryptic end and to contain the TEV modification. ProLUCID data was filtered through DTASelect to achieve a peptide false-positive rate below 1%.

Thiolase activity assay.

Enzymatic activity of Acaa1b and Acaa2 was performed using the Fluorometric Acetyltransferase Activity Assay Kit (ABCAM ab204536). The assay was performed per the protocol with 4 μg pure protein and 100 nM acetoacetyl-CoA (Sigma A1625), fluorescence was measured at 380/520 ex/em on a SpectraMax i3x detection platform.

Metabolomic profiling.

Lipidomic profiling was performed as previously described[12,17]. Nonpolar lipid metabolites from the liver of *in vivo*-treated mice or HepG2 cells were extracted in 3 ml of 2:1 chloroform:methanol and 1 ml of PBS with inclusion of internal standards dodecylglycerol (10 nmol, Santa Cruz Biotechnology) and pentadecanoic acid (10 nmol, Sigma-Aldrich). Organic and aqueous layers were separated by centrifugation at 1000×g for 5 min and the organic layer was collected, dried under a stream of nitrogen and dissolved in 120 μl chloroform. Metabolites were separated by liquid chromatography as previously described[17,18]. Metabolomes were separated using reverse-phase chromatography with a Luna C5 column (50 mm × 4.6 mm with 5 μm diameter particles, Phenomenex). Mobile phase A consisted of 95:5 ratio of water/methanol and mobile phase B consisted of 2-propanol, methanol, and water in a 60:35:5 ratio. Solvent modifiers 0.1 % formic acid with 5 mM ammonium formate and 0.1 % ammonium hydroxide were used to assist ion formation as well as to improve the LC resolution in both positive and negative ionization modes, respectively. The flow rate for each run started at 0.1 ml/min for 5 min to alleviate backpressure associated with injecting chloroform. The gradient started at 0 % B and increased linearly to 100 % B over the course of 45 min with a flow rate of 0.4 ml/min, followed by an isocratic gradient of 100 % B for 17 min at 0.5 ml/min before equilibrating for 8 min at 0 % B with a flow rate of 0.5 ml/min.

MS analysis was performed with an electrospray ionization (ESI) source on an Agilent 6430 QQQ LC-MS/MS (Agilent Technologies). The capillary voltage was set to 3.0 kV, and the fragmentor voltage was set to 100 V. The drying gas temperature was 350°C, the drying gas flow rate was 10 l/min, and the nebulizer pressure was 35 psi. Metabolites were identified by SRM of the transition from precursor to product ions at associated optimized collision energies and retention times as previously described[17,18]. Metabolites were quantified by integrating the area under the curve, and then normalized to internal standard values and for livers, tissue weight in mg. Metabolite levels are expressed as relative abundances as compared to controls.

HepG2 FAO Seahorse studies.

HepG2 cells were plated into XF24 cell culture plates (50,000 cells per well, 500 μl substrate-limited DMEM per well, Seahorse Biosciences) overnight. 120 min before starting the assay, 1 mM AC or DMSO were added to their respective wells. The culture medium was removed from each well and replaced with FAO medium (375 μl) containing 1 mM AC or DMSO 45 min before starting the assay. 15 min prior to the start of the assay, etomoxir (40 μM final, Abcam, Inc. #144763) was added to its respective wells. Cells were incubated in a CO_2-free incubator at 37 °C for 45 min. Prior to the rate measurements, Palmitate:BSA or BSA control (87.5 μl per well, Seahorse Biosciences #102720–100) were added to all of

the wells. The XF Instrument (Seahorse Biosciences) gently mixed the assay media in each well for 10 min to allow the oxygen partial pressure to reach equilibrium. The oxygen consumption rate (OCR) and extracellular acidification rate (ECAR) were measured simultaneously three times to establish a baseline rate. For each measurement, with a total of 12 measurements, there was a 3 min mix followed by 3 min wait time to restore normal oxygen tension and pH in the microenvironment surrounding the cells. Drug injection was performed throughout the assay. Oligomycin (2.5 μg/ml final) was injected after measurement 3, FCCP (0.5 μM final) was injected after measurement 6, and rotenone/antimycin A (2 and 4 μM final, respectively) after measurement 9.

Supplementary Material

Refer to Web version on PubMed Central for supplementary material.

Acknowledgements

We thank the UC Davis Proteomics Core for MS-based proteomics detection. This work was supported by the Searle Scholar Award, the Center for Environmental Research on Toxics, the National Institutes of Health (P42ES004705), the American Cancer Society Research Scholar Award (RSG-14-242-01-TBE), a National Science Foundation Graduate Fellowship (JLC), and a National Institutes of Health Training grant (5T32DK061918-13) (JLC).

References

(1). Grube A, Donaldson D, Kiely T, and Wu L (2011, 2) Pesticides Industry Sales and Usage: 2006 and 2007 Market Estimates. EPA United States Environmental Protection Agency.

(2). (2006, March) Report of the Food Quality Protection Act (FQPA) Tolerance Reassessment Progress and Risk Management Decision (TRED) for Acetochlor. Environmental Protection Agency.

(3). Pace NJ, and Weerapana E (2013) Diverse functional roles of reactive cysteines. ACS Chem. Biol 8, 283–296. [PubMed: 23163700]

(4). Counihan JL, Ford B, and Nomura DK (2015) Mapping proteome-wide interactions of reactive chemicals using chemoproteomic platforms. Curr. Opin. Chem. Biol 30, 68–76. [PubMed: 26647369]

(5). Roberts AM, Ward CC, and Nomura DK (2016) Activity-based protein profiling for mapping and pharmacologically interrogating proteome-wide ligandable hotspots. Curr. Opin. Biotechnol 43, 25–33. [PubMed: 27568596]

(6). Haapalainen AM, Meriläinen G, and Wierenga RK (2006) The thiolase superfamily: condensing enzymes with diverse reaction specificities. Trends Biochem. Sci 31, 64–71. [PubMed: 16356722]

(7). Mizuno Y, Ninomiya Y, Nakachi Y, Iseki M, Iwasa H, Akita M, Tsukui T, Shimozawa N, Ito C, Toshimori K, Nishimukai M, Hara H, Maeba R, Okazaki T, Alodaib ANA, Al Amoudi M, Jacob M, Alkuraya FS, Horai Y, Watanabe M, Motegi H, Wakana S, Noda T, Kurochkin IV, Mizuno Y, Schönbach C, and Okazaki Y (2013) Tysnd1 deficiency in mice interferes with the peroxisomal localization of PTS2 enzymes, causing lipid metabolic abnormalities and male infertility. PLoS Genet. 9, e1003286. [PubMed: 23459139]

(8). Lee J, Choi J, Scafidi S, and Wolfgang MJ (2016) Hepatic Fatty Acid Oxidation Restrains Systemic Catabolism during Starvation. Cell Rep. 16, 201–212. [PubMed: 27320917]

(9). Klipsic D, Landrock D, Martin GG, McIntosh AL, Landrock KK, Mackie JT, Schroeder F, and Kier AB (2015) Impact of SCP-2/SCP-x gene ablation and dietary cholesterol on hepatic lipid accumulation. Am. J. Physiol. Gastrointest. Liver Physiol 309, G387–399. [PubMed: 26113298]

(10). Kim T, Moore JF, Sharer JD, Yang K, Wood PA, and Yang Q (2014) Carnitine Palmitoyltransferase 1b Deficient Mice Develop Severe Insulin Resistance After Prolonged High Fat Diet Feeding. J. Diabetes Metab. 5.

(11). Lee J, Choi J, Aja S, Scafidi S, and Wolfgang MJ (2016) Loss of Adipose Fatty Acid Oxidation Does Not Potentiate Obesity at Thermoneutrality. Cell Rep. 14, 1308–1316. [PubMed: 26854223]

(12). Medina-Cleghorn D, Bateman LA, Ford B, Heslin A, Fisher KJ, Dalvie ED, and Nomura DK (2015) Mapping Proteome-Wide Targets of Environmental Chemicals Using Reactivity-Based Chemoproteomic Platforms. Chem. Biol 22, 1394–1405. [PubMed: 26496688]

(13). Weerapana E, Wang C, Simon GM, Richter F, Khare S, Dillon MBD, Bachovchin DA, Mowen K, Baker D, and Cravatt BF (2010) Quantitative reactivity profiling predicts functional cysteines in proteomes. Nature 468, 790–795. [PubMed: 21085121]

(14). Backus KM, Correia BE, Lum KM, Forli S, Horning BD, González-Páez GE, Chatterjee S, Lanning BR, Teijaro JR, Olson AJ, Wolan DW, and Cravatt BF (2016) Proteome-wide covalent ligand discovery in native biological systems. Nature 534, 570–574. [PubMed: 27309814]

(15). Speers AE, Adam GC, and Cravatt BF (2003) Activity-based protein profiling in vivo using a copper(i)-catalyzed azide-alkyne [3 + 2] cycloaddition. J. Am. Chem. Soc 125, 4686–4687. [PubMed: 12696868]

(16). Xu T, Park SK, Venable JD, Wohlschlegel JA, Diedrich JK, Cociorva D, Lu B, Liao L, Hewel J, Han X, Wong CCL, Fonslow B, Delahunty C, Gao Y, Shah H, and Yates JR (2015) ProLuCID: An improved SEQUEST-like algorithm with enhanced sensitivity and specificity. J. Proteomics 129, 16–24. [PubMed: 26171723]

(17). Louie SM, Grossman EA, Crawford LA, Ding L, Camarda R, Huffman TR, Miyamoto DK, Goga A, Weerapana E, and Nomura DK (2016) GSTP1 Is a Driver of Triple-Negative Breast Cancer Cell Metabolism and Pathogenicity. Cell Chem. Biol 23, 567–578. [PubMed: 27185638]

(18). Benjamin DI, Cozzo A, Ji X, Roberts LS, Louie SM, Mulvihill MM, Luo K, and Nomura DK (2013) Ether lipid generating enzyme AGPS alters the balance of structural and signaling lipids to fuel cancer pathogenicity. Proc. Natl. Acad. Sci. U. S. A 110, 14912–14917. [PubMed: 23980144]

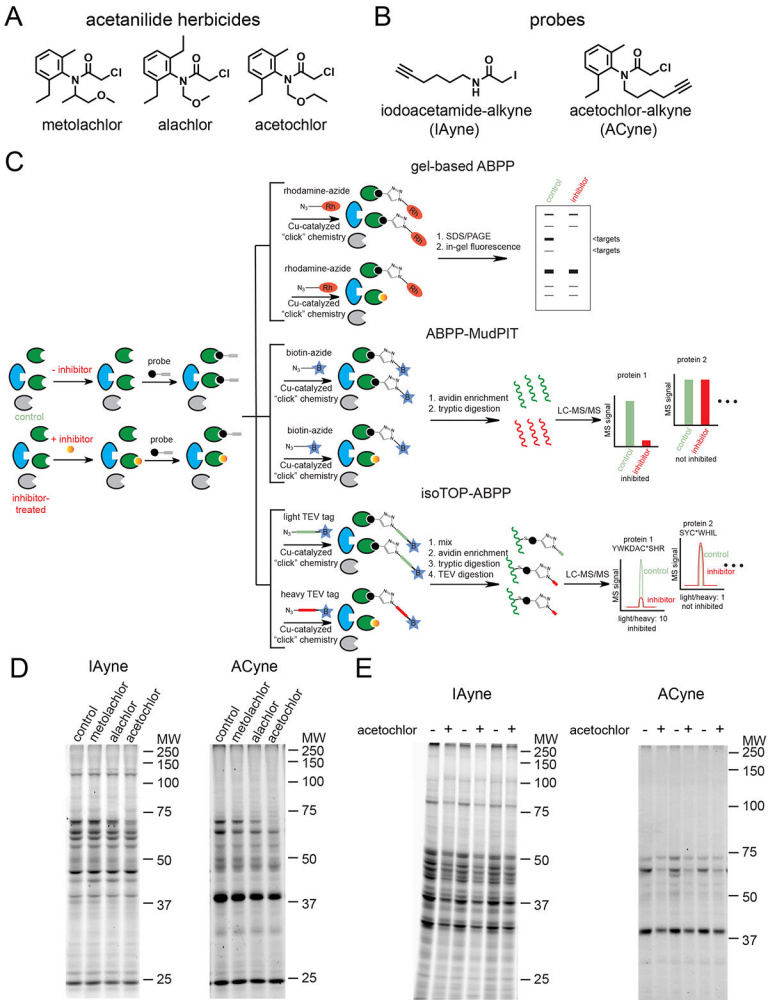

Figure 1. Assessing acetanilide herbicide reactivity using ABPP platforms.

(A) Structures of acetanilide herbicides. **(B)** Structures of the broad cysteine-reactive probe iodoacetamidealkyne (IAyne) and acetochlor-alkyne (ACyne). **(C)** ABPP platforms used in this study. Acetanilide herbicides were treated either *in vitro* or *in vivo* followed by treatment of liver proteomes with either IAyne or ACyne probes. IAyne and ACyne reactivity and acetanilide herbicide targets were subsequently determined either by fluorescence using gel-based ABPP, by protein pull-down by ABPP-MudPIT, or by mapping site-of-modification using isoTOP-ABPP. **(D)** Acetanilide herbicide reactivity *in vitro* in mouse liver proteome using gel-based ABPP. Proteomes were pre-treated *in vitro* (30 min) with metolochlor, alachlor, or AC, and then labeled with IAyne labeling (10 μM, 60 min) or ACyne labeling (1 μM, 60 min) followed by conjugation of rhodamine-azide by click-chemistry, and visualization of IAyne or ACyne reactivity by SDS/PAGE and in-gel fluorescence. **(E)** AC reactivity *in vivo* in mouse liver proteome using gel-based ABPP. Mice were pre-treated *in vivo* with AC (85 mg/kg ip, 4 h), and mouse liver proteomes were subsequently labeled *ex vivo* with IAyne (10 μM, 60 min) or ACyne (1 μM, 60 min), followed by rhodamine conjugation, SDS/PAGE, and in-gel fluorescence. Gels in **(D)** and **(E)** are representative gels from n=3.

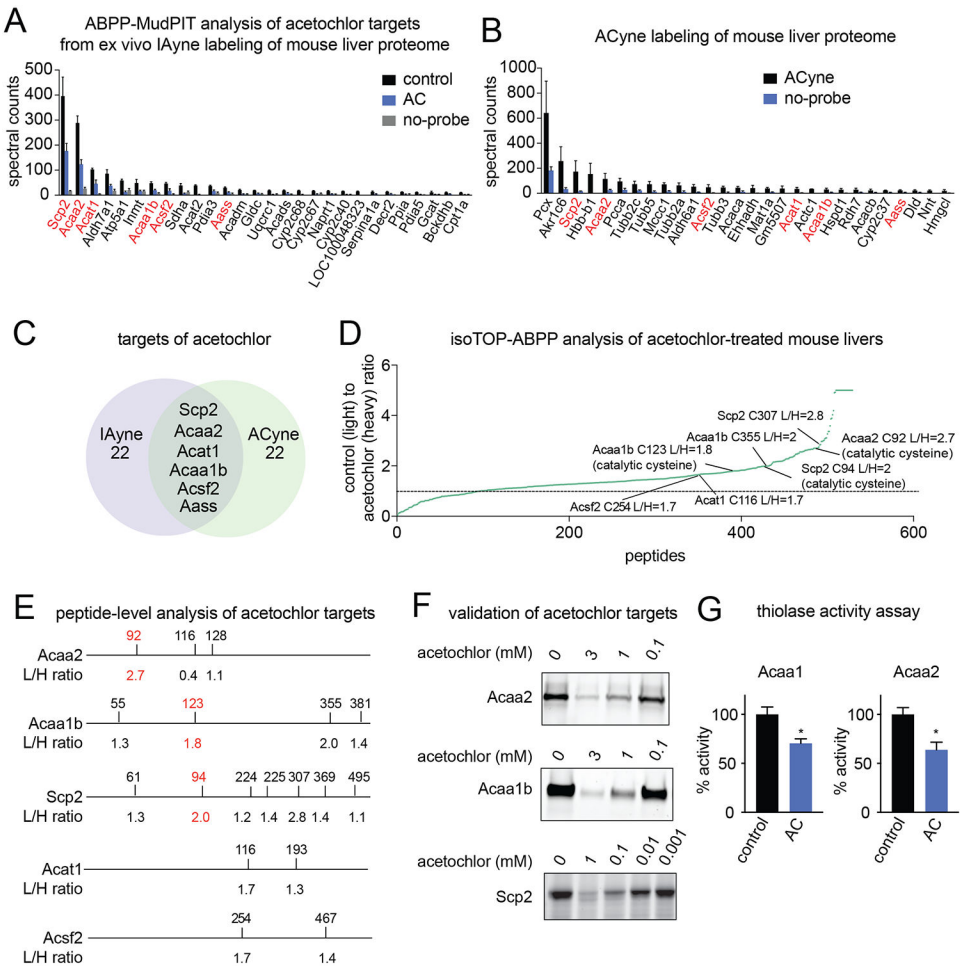

Figure 2. Mapping *in vivo* targets of AC in mouse liver using ABPP platforms.

(A) ABPP-MudPIT analysis of AC targets *in vivo*. Mice were treated *in vivo* with vehicle or AC (85 mg/kg ip, 4 h) and mouse liver proteomes were labeled with IAyne *ex vivo* (10 μM, 30 min) or DMSO (no-probe control), followed by conjugation of biotin-azide by click-chemistry, avidin-enrichment and MudPIT analysis. Shown are targets that showed significant ($p<0.05$) and >50 % reduction in IAyne labeling in AC-treated groups compared to vehicle-treated controls that also showed >2-fold IAyne enrichment in vehicle-treated compared to no-probe controls. **(B)** ACyne targets in mouse liver proteome. Mouse liver proteomes were labeled with ACyne (1 μM, 30 min) or DMSO (no-probe control), and subsequently conjugated to biotin-zide, avidin-enriched, and analyzed by MudPIT. Shown are targets that showed significant ($p<0.05$) and >2-fold ACyne enrichment compared to no-probe controls. **(C)** Experiments in **(A)** and **(B)** each yielded 28 targets of AC, of which 6 were overlapping. **(D)** isoTOP-ABPP analysis of *in vivo* AC targets. *In vivo* vehicle or AC (85 mg/kg ip, 4h)-treated mouse liver proteomes were labeled with IAyne, followed by conjugation of biotin-azide bearing an isotopically light (vehicle-treated) or heavy (AC-treated) tag and TEV protease recognition sequence, vehicle and treated groups were combined in a 1:1 ratio, avidin-enriched, tryptically digested, and probe-modified tryptic peptides were avidin-enriched again and released by TEV protease digestion. Probe-

modified light or heavy tryptic peptides were analyzed by MudPIT. A larger light to heavy ratio indicates that AC bound to a particular cysteine on that peptide. **(E)** Specific cysteines on Acaa2, Acaa1b, Scp2, Acat2, and Acsf2 labeled by IAyne and their light to heavy ratios determined from isoTOP-ABPP studies in **(D)**. Highlighted in red are catalytic cysteines. **(F)** Validation of AC binding to thiolase enzymes. AC was pre-incubated for 30 min with either overexpressed mouse protein in HEK293T cells or pure mouse protein and labeled with IAyne (10 μM, 30 min), followed by conjugation of rhodamine-azide, SDS/PAGE, and in-gel fluorescence. Gels are representative of n=3. **(G)** Thiolase activity assays. DMSO or AC (1 mM, 30 min) was incubated with pure mouse Acaa1 and Acaa2 protein and thiolase activity was measured using a substrate assay. Data in **(A, B, G)** are presented as mean ± sem, n=3. Significance in (G) is presented as *$p<0.05$ compared to DMSO-treated control.

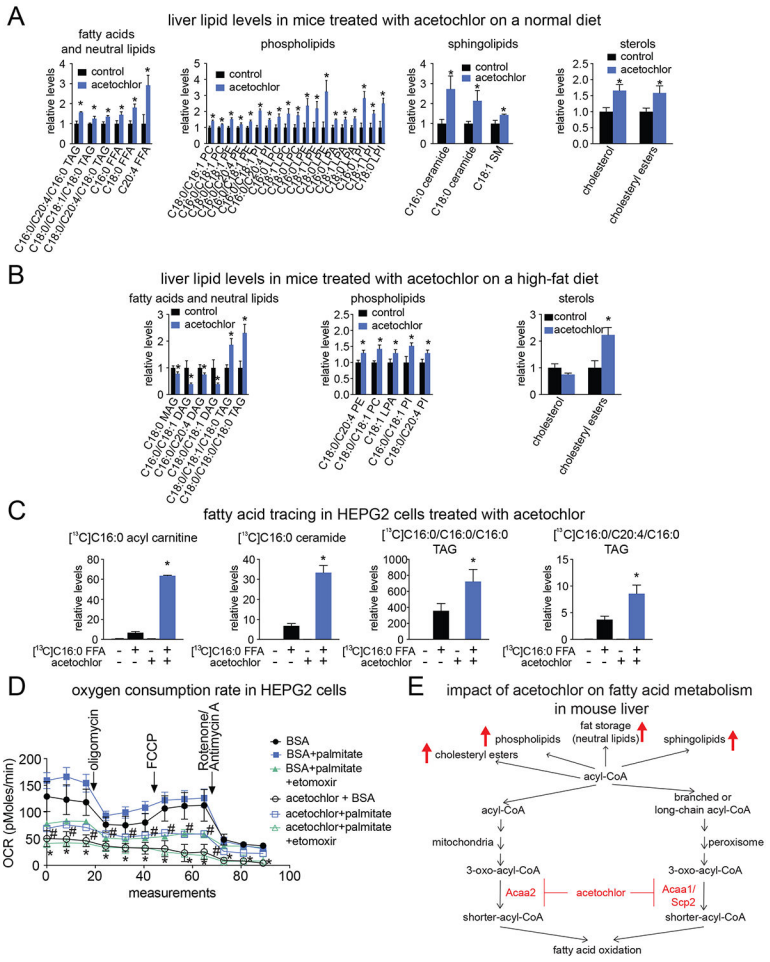

Figure 3. AC inhibits fatty acid oxidation in mouse liver leading to lipid dysregulation.

(A, B) Liver lipid levels in mice treated with AC. Mice were treated with vehicle or AC (85 mg/kg ip, once per day for 6 days) on a chow diet **(A)** or vehicle or AC (85 mg/kg ip once every other day for 6 weeks) on a high-fat diet **(B)**. High-fat diet was initiated 4 weeks before initiation of AC treatments. Single-reaction monitoring (SRM)-based targeted LC-MS/MS metabolomic profiling was performed on livers. Shown are representative metabolites that were significantly (*$p < 0.05$) altered in livers from mice treated with AC compared to vehicle-treated controls. Abbreviations: FFA, free fatty acid; TAG, triacylglycerols; DAG, diacylglycerol; MAG, monoacylglycerol; PC, phosphatidylcholine; PE, phosphatidylethanolamine; PI, phosphatidyl inositol; PA, phosphatdic acid; SM, sphingomyelin. “L” denotes lyso. **(C)** Isotopic fatty acid tracing in HepG2 hepatocyte cells treated with AC. HepG2 cells were pre-treated with DMSO vehicle or AC (1 mM, 1 h) before labeling cells with [U-^{13}C]palmitic acid ([^{13}C]C16:0 free fatty acid (FFA)) (10 μM, 6 h). Isotopic incorporation of [^{13}C]C16:0 FFA into complex lipids was measured by SRM-based LC-MS/MS. **(D)** Oxygen consumption rate (OCR) in HepG2 cells pre-treated with AC (1 mM, 2 h). Etomoxir (40 μM) was added 15 min prior to the start of the experiment to ensure that CPT-1 was inhibited. BSA control or BSA;Palmitate (87.5 μL) were added immediately before the start of the experiment. Oligomycin (2.5 ug/ml) was added between measurements 3 and 4, FCCP (0.5 μM) was added between 6 and 7, and rotenone and

antimycin A (2 and 4 μM, respectively) were added between 9 and 10, with 12 measurements total. **(E)** AC inhibits fatty acid oxidation enzymes, leading to impaired fatty acid oxidation and diversion of fatty acids into other lipid pathways. Data in **(A-D)** are presented as mean ± sem, n=5 per group for (A-C) and n=4 for (D). Significance is presented as *p<0.05 compared to vehicle-treated controls in **(A-C)**. Significance in **(D)** is presented as *p<0.05 comparing BSA groups to AC + BSA groups and #p<0.05 comparing BSA+palmitate to AC + palmitate.